HHS Public Access

Author manuscript

*Biochem J.* Author manuscript; available in PMC 2020 November 12.

Published in final edited form as:

*Biochem J.* ; 476(12): 1791–1803. doi:10.1042/BCJ20190108.

# The histidine-rich loop in the extracellular domain of ZIP4 binds zinc and plays a role in zinc transport

**Tuo Zhang**[1,*], **Eziz Kuliyev**[2,*], **Dexin Sui**[1], **Jian Hu**[1,2]

[1]Department of Biochemistry and Molecular Biology, Michigan State University, East Lansing, MI, U.S.A.;

[2]Department of Chemistry, Michigan State University, East Lansing, MI, U.S.A.

## Abstract

The Zrt-/Irt-like protein (ZIP) family mediates zinc influx from extracellular space or intracellular vesicles/organelles, playing a central role in systemic and cellular zinc homeostasis. Out of the 14 family members encoded in human genome, ZIP4 is exclusively responsible for zinc uptake from dietary food and dysfunctional mutations of ZIP4 cause a life-threatening genetic disorder, Acrodermatitis Enteropathica (AE). About half of the missense AE-causing mutations occur within the large N-terminal extracellular domain (ECD), and our previous study has shown that ZIP4–ECD is crucial for optimal zinc uptake but the underlying mechanism has not been clarified. In this work, we examined zinc binding to the isolated ZIP4–ECD from *Pteropus Alecto* (black fruit bat) and located zinc-binding sites with a low micromolar affinity within a histidine-rich loop ubiquitously present in ZIP4 proteins. Zinc binding to this protease-susceptible loop induces a small and highly localized structural perturbation. Mutagenesis and functional study on human ZIP4 by using an improved cell-based zinc uptake assay indicated that the histidine residues within this loop are not involved in preselection of metal substrate but play a role in promoting zinc transport. The possible function of the histidine-rich loop as a metal chaperone facilitating zinc binding to the transport site and/or a zinc sensor allosterically regulating the transport machinery was discussed. This work helps to establish the structure/function relationship of ZIP4 and also sheds light on other metal transporters and metalloproteins with clustered histidine residues.

## Introduction

Cellular zinc homeostasis is achieved by co-ordinated actions of zinc transporters, zinc buffer proteins/molecules, zinc storage proteins and zinc utilizing proteins. In humans, there are two primary zinc transporters families: the ZnT family transports zinc out of cells against electrochemical gradient, whereas the Zrt-/Irt-like protein (ZIP) family mediates zinc influx

**Correspondence:** Jian Hu (hujian1@msu.edu).

*These authors contributed equally to this work.

Author Contribution

J.H. formulated the project. T.Z., E.K. and D.S. conducted experiments. All the authors participated in data analysis and discussion. J.H., T.Z. and E.K. wrote the manuscript.

Competing Interests

The Authors declare that there are no competing interests associated with the manuscript.

along the gradient from either extracellular space or intracellular vesicles/organelles [1–4]. Out of the 14 ZIPs encoded in human genome, ZIP4 is specifically expressed in gastrointestinal system where it plays an essential role in zinc uptake from dietary food [1] and also in kidney where it is postulated to be involved in zinc reabsorption from urine. Aberrant overexpression of ZIP4 in several types of cancers has been reported [5–8], whereas dysfunctional mutations of ZIP4 cause a rare autosomal recessive genetic disorder, Acrodermatitis Enteropathica (AE), due to severe zinc deficiency [9–11], which is characterized by inflammation of the skin, hair loss and diarrhea. Although there is no cure for the inherited form of AE and the patients may die without treatment, lifelong dietary zinc supplement can efficiently relieve the symptom. Markedly, about half of AE-causing mutations occur within the extracellular domain (ECD), suggestive of a key role in ZIP4 function. Our previous study has shown that deletion of the ECD reduces zinc transport activity of ZIP4 by 75% [12], indicating that although ZIP4–ECD is not absolutely required for ZIP4 function, it is crucial for optimal zinc transport. Besides its role in promoting zinc transport, ZIP4–ECD was also suggested to be involved in zinc sensing. For instance, it has been reported that an AE-causing mutation in the ECD largely abolished zinc-elicited endocytosis [13]. Another report showed that several AE-causing mutations in the ECD affected ZIP4 proteolysis triggered by zinc deficiency [14]. Since there are many conserved metal-chelating residues (cysteine, histidine, glutamate and aspartate) in ZIP4–ECD, it was suggested that these residues are potentially involved in zinc binding [14]. In the structure of ZIP4–ECD from *Pteropus Alecto* (pZIP4–ECD) [12], it was found that all the eight invariant cysteine residues formed four disulfide bonds. Based on the crystal structure of a prokaryotic ZIP [15] and a coevolution-based computational model [16], we generate a human ZIP4 structure model (Figure 1A) where the histidine-rich loop in the ECD is in close proximity to the transport entrance and forms a potential zinc-binding site. Although sequence alignment across several closely related species indicates that this segment is highly variable (Figure 1B), the clustered histidine residues is a common feature of ZIP4, suggestive of a certain function.

In this work, we demonstrated that the histidine residues in the His-rich loop form the primary zinc-binding sites of pZIP4–ECD, and zinc binding to this highly dynamic and protease-susceptible loop induces a small and localized conformational change. Mutagenesis and functional assays on human ZIP4 showed that this loop is not involved in substrate selection, but plays a role in promoting zinc transport, partially accounting for the function of ZIP4–ECD.

## Materials and methods

### Protein expression and purification

pZIP4–ECD (gene ID: ELK11751) was expressed and purified in the same way as reported [12]. Briefly, the expression of pZIP4–ECD in the *E.coli* strain of Origami™ B(DE3) pLysS (Novagen) was induced by 0.2 mM IPTG in lysogeny broth medium. After cell lysis by sonication, pZIP4–ECD was purified using nickel-nitrilotriacetic acid column. The N-terminal $His_6$-tag was removed by thrombin, and then the protein (treated by 10 mM EDTA) was further purified by ion exchange chromatography on a Mono-Q column (GE

Healthcare), followed by size-exclusion chromatography (GE Healthcare) in the buffer containing 10 mM HEPES, pH 7.3 and 100 mM NaCl or 10 mM Tris–$H_2SO_4$, pH 7.0. The mutants were purified in the same way. Inductively coupled plasma mass spectrometry experiment confirmed the purified protein is in apo form (Supplementary Table S1).

## Fluorescence titration

To determine the dissociation constant towards zinc ions, FluoZin-1 (Thermo Fisher Scientific) was dissolved in a buffer containing 50 mM HEPES pH 7.3, 100 mM NaCl at the concentration of 5 μM, and titrated with the indicated concentration of $ZnCl_2$. The fluorescence spectra were recorded at 25°C in a 0.5 cm × 1 cm quartz cuvette in the same buffer. The fluorescence was excited at the wavelength of 490 nm and the spectra were recorded in the range of 500–650 nm (Cary Eclipse Fluorescence Spectrophotometer, Agilent). The excitation and emission slits were set to 2.5 and 5 nm, respectively. For the competition titration, 10 μM apo form pZIP4–ECD was mixed with 5 μM FluoZin-1 in the same buffer and titration was performed in the same way. Free zinc concentrations were calculated using the recorded fluorescence intensity and the determined apparent $K_d$ of FluoZin-1, and zinc occupancies (the number of bound zinc ions per protein molecule) were calculated using the followed equations:

$$T_{Zn} = [Zn] + [Zn \cdot Dye] + [Zn \cdot P] \quad (1)$$

$$T_{Dye} = [\,Dye\,] + [Zn \cdot \,Dye\,] \quad (2)$$

$$T_P = [P] + [Zn \cdot P] \quad (3)$$

$$K_{d,\,Dye} = [Zn] \times [\,Dye\,]/[Zn \cdot \,Dye\,] \quad (4)$$

$$F/F_{max} = [Zn \cdot \,Dye\,]/T_{Dye} \quad (5)$$

$$\text{Occupancy} = [Zn \cdot P]/T_P \quad (6)$$

Where $T_{Zn}$: total Zn concentration, $T_{Dye}$: total FluoZin-1 concentration, $T_p$: total protein concentration, [Zn]: free $Zn^{2+}$ concentration, [Dye]: free FluoZin-1 concentration, [P]: apo form protein concentration, [Zn·Dye]: Zn-FluoZin-1 complex concentration, and [Zn·P]: Zn–protein complex concentration, $K_d$: dissociation constant, $F/F_{max}$: normalized fluorescence change. $F_{max}$ was measured by adding zinc up to 1 mM at the end of the titration. The fluorescence intensities have been calibrated to compensate volume change during titration. To obtain apparent dissociation constant, occupancy ($y$) was plotted against free zinc concentration ($x$) and then curve fitting was conducted using the Hill model (OriginPro 8.5):

$$y = B_{\max} \times x^n / \left(K_d^n + x^n\right) \quad (7)$$

where $B_{max}$ is the number of binding sites and the Hill coefficient ($n$) indicates the cooperation among the binding sites. To estimate the averaged apparent dissociation constants of the first two zinc-binding sites, $B_{max}$ was set at 2 and only the data with free zinc concentration below 3 μM were used to minimize the effects of additional low-affinity zinc-binding sites on curve fitting.

## Cell culture and transfection

Human embryonic kidney cells (HEK293T, ATCC) were cultured in Dulbecco's modified Eagle medium (DMEM, Invitrogen) supplemented with 10% (v/v) fetal bovine serum (Invitrogen) and Gibco Antibiotic–Antimycotic (Invitrogen). Zinc depletion medium was prepared using Chelex 100 (Bio-Rad). A suspension of 1.3% (w/v) Chelex 100 beads in DMEM medium supplemented with 10% fetal bovine serum was incubated at 4°C for 2 h with a constant gentle shake, followed by filtration of the supernatant through a 0.22 μm filter. Cells were seeded on 24-wells trays for 16 h in basal medium, followed by transiently transfection with an expression vector containing human ZIP4 gene (gene ID: BC062625) by the Lipofectamine 2000 reagent (Invitrogen). Cells were allowed to grow for another 36 h before $^{65}Zn$ uptake and ZIP4 surface expression assays.

## Trypsin proteolysis

To optimize the partial proteolysis condition, 2 μl of trypsin dissolved in water with variable stock concentrations was added into 18 μl pZIP4–ECD (0.15 mg/ml in 10 mM Tris–$H_2SO_4$, pH 7.0). After incubation at room temperature for 20 min, the reaction was stopped by adding 6 μl of SDS–PAGE loading buffer containing 1 mM PMSF. To test the effects of zinc ions on partial proteolysis, the reaction was performed in the presence of different concentrations of $ZnSO_4$ at the optimized protein:trypsin ratio (300 : 1, m/m). Partial proteolysis was analyzed by SDS–PAGE.

## Mass spectrometry of pZIP4–ECD and its proteolytic fragments

The unprocessed and fully processed pZIP4–ECD by trypsin in 10 mM Tris–$H_2SO_4$, pH 7.0 were analyzed using a Waters G2-XS quadrupole-time-of-flight mass spectrometer using electrospray ionization (ESI–TOF–MS) operating in positive ion mode and scanning a mass range of $m/z$ 200–2000 with 1 scan per second. Protein mass spectra were deconvoluted using the MaxEnt algorithm in the Waters Masslynx software package.

## Circular dichroism

The circular dichroism (CD) spectra of 6 μM pZIP4–ECD or the mutant in 10 mM Tris–$H_2SO_4$ (pH 7.0) were recorded in a 1 mm quartz cuvette by using a Chirascan™ CD Spectrometer. Concentrations of the proteins were measured by using a NanoDrop ND-1000 Spectrophotometer. In zinc titration, aliquots of 3.75 μl $ZnSO_4$ were sequentially added into 300 μl protein samples. The $ZnSO_4$ stock solutions were made in water without buffer or any other salt. After adding $ZnSO_4$, the samples were allowed to balance at room temperature for 5 min before the spectra were scanned. Three scans were recorded and

averaged at each step. The CD spectra were analyzed using the K2D3 server at http://cbdm-01.zdv.uni-mainz.de/~andrade/k2d3/n.

### Intrinsic tryptophan fluorescence titration

Intrinsic tryptophan fluorescence spectra of 2 μM pZIP4–ECD or the mutant in 10 mM Tris–$H_2SO_4$ (pH 7.0) were recorded in a 10 mm quartz cuvette by using a Varian Cary Eclipse Fluorescence Spectrophotometer. Aliquots of 2.8 μl of $ZnSO_4$ were sequentially added into the cuvette containing 700 μl protein sample. Excitation wavelength was 295 nm and ex/em slits were set to 5 nm/5 nm. After adding $ZnSO_4$, the samples were allowed to balance at room temperature for 5 min before the spectra were recorded in the range of 310–410 nm. Three scans were averaged at each step. Zinc titration to the wild-type pZIP4–ECD in the presence of 10 mM EDTA was conducted in the same way.

### $^{65}$Zinc uptake assay

HEK293T cells were washed by zinc uptake buffer (10 mM HEPES pH 7.3, 142 mM NaCl, 10 mM Glucose, 5 mM KCl) and then incubated with the indicated concentration of $ZnCl_2$ (containing 40% $^{65}ZnCl_2$) in the Chelex-treated media at 37°C for 20 min with occasional gentle shaking. Uptake was stopped by adding the same volume of stop buffer (ice-cold zinc uptake buffer with 1 mM EDTA) and cells were collected into Eppendorf tubes on ice. Cells were gently washed two times by zinc uptake buffer and lysed in 0.5% Triton X-100. Cell-associated radioactivity was measured with a Packard Cobra Auto-Gamma γ-counter and the amount of zinc was calculated using a standard $^{65}$Zn radioactivity curve. The cells transfected with the vector without inserted ZIP4 gene (empty vector) were treated in the same way and used as control in the assay. The amount of zinc transported into the cells through hZIP4 was calculated by subtracting the zinc uptake in control cells from the zinc uptake in the cells transfected with hZIP4–HA. The zinc uptake rate is expressed as pmol $min^{-1}$ $mg^{-1}$ protein and the total protein concentrations in the samples were measured using Bradford method (Bio-Rad). The zinc uptake data were firstly calibrated with the surface expression level and then fitted using the Michaelis–Menten equation. Metal selectivity of hZIP4 was carried out with 10 μM $ZnCl_2$ (containing 40% $^{65}ZnCl_2$) plus non-radioactive $ZnCl_2$, $CaCl_2$, $MgCl_2$, $CoCl_2$, $NiCl_2$, $CuSO_4$ and $MnCl_2$ at 200 μM, 2 mM, 20 mM, 200 μM, 200 μM, 200 μM and 200 μM, respectively. The same experiment was also conducted in the presence of 200 μM $FeSO_4$ and 1 mM ascorbic acid. Each individual experiment included three repeats, and statistical significance was tested with the Student's *t*-test.

### hZIP4–HA surface expression assay

hZIP4–HA expressed at the plasma membrane was indicated by the surface-bound anti-HA antibodies recognizing the C-terminal HA tag of hZIP4. After washing twice with Dulbecco's phosphate-buffered saline (DPBS), cells were fixed for 5 min in 4% formaldehyde at room temperature. Cells were then washed three times in DPBS and incubated with 3 μg/ml anti-HA antibody (Invitrogen) diluted with 5% BSA in DPBS for 2 h at room temperature. Cells were washed five times with DPBS to remove unbound antibodies and then lysed in SDS–PAGE loading buffer. The anti-HA antibody bound to the surface hZIP4–HA in cell lysates was detected in Western blot with HRP-conjugated goat anti-mouse immunoglobulin-G (1 : 2500). As a loading control, β-actin levels were detected

using an anti-β-actin antibody (1 : 2500) followed by a goat anti-rabbit immunoglobulin-G (1 : 3000) by chemiluminescence. All antibodies were purchased from Cell Signaling Technology unless indicated otherwise.

## Results

### The primary zinc-binding sites in pZIP4–ECD are located within the His-rich loop

To test zinc binding to ZIP4–ECD, we conducted zinc titration in the presence of a zinc-specific fluorescence probe, FluoZin-1, of which fluorescence intensity increases upon zinc binding [17]. Zinc-specific fluorescence probes have been used in estimating zinc-binding affinity of a variety of proteins through competition titration [18,19]. As shown in Supplementary Figure S1A, we firstly measured the zinc-binding affinity of FluoZin-1 under our experimental condition. After curve fitting using the one-site model, we obtained an apparent dissociation constant ($K_d$) of 29 μM, which is larger than the reported value (8 μM). We reason that salt included in the buffer reduced zinc binding to FluoZin-1. We then included the purified pZIP4–ECD in apo form as a zinc competitor in titration (Figure 2). The zinc-binding curve of FluoZin-1 was significantly right-shifted and there was only very small fluorescence increase at the beginning of the titration, indicating that pZIP4–ECD binds zinc ions with an affinity much higher than FluoZin-1. By using the experimentally determined apparent $K_d$ of FluoZin-1 and the fluorescence intensities measured during titration, we calculated and plotted the number of bound zinc ion per protein (zinc occupancy) against free zinc concentration. Curve fitting using the Hill model allowed us to estimate the averaged dissociation constant (0.62 μM) for the first two zinc-binding sites (Supplementary Figure S1B, see details in Materials and methods).

To locate the metal binding sites in pZIP4–ECD, we tried to obtain the co-structure by either co-crystallization or soaking the apo protein crystals with zinc ions, but these trials failed due to lack of crystal in the presence of zinc or destroyed crystal lattice upon zinc soaking. Potential metal binding sites can be identified by manually checking the apo form structure (Supplementary Figure S2), but none of them, except for the His-rich loop (Figure 1), contains more than one histidine residue which is highly preferred for zinc ion binding. We then focused on the His-rich loop of pZIP4–ECD, which contains four clustered histidine residues (H234, H237, H238 and H239). To examine their roles in zinc binding, we mutated all the histidine residues into serine residues (the 4HS mutant). Compared with alanine, serine was chosen to preserve hydrophilicity, which would produce less structural disturbances caused by mutations. Indeed, the CD spectrum of the purified 4HS mutant is essentially the same as that of the wild-type pZIP4–ECD (Supplementary Figure S3). As shown in Figure 2, the 4HS mutant protein barely shifted the zinc-binding curve of FluoZin-1, indicating that the primary high-affinity zinc-binding sites have been eliminated by the mutations. This result unambiguously demonstrated that the primary zinc-binding sites of pZIP4–ECD are only present in the His-rich loop. Similar to the 4HS mutant, the H237S/H238S/H239S triple mutant (the 3HS mutant) only slightly shifted the zinc-binding curve, indicating that a single histidine residue (H234) is not adequate to support zinc binding with low micromolar affinity. To further dissect the role of each histidine residue, we made four His-to-Ser single mutations (H234S, H237S, H238S and H239S) and tested

zinc binding under the same condition (Figure 2). The results showed that, when compared with the wild-type protein, the mutants caused a smaller right-shift of the zinc-binding curve, suggestive of reduced zinc-binding affinity (Supplementary Figure S1B). Therefore, the four histidine residues are all contributive to zinc binding and their effects appear to be additive. It is plausible that there is no defined zinc-binding mode in the His-rich loop. Instead, as suggested in a recent NMR study of the intracellular His-rich loop of hZIP4 [20], the zinc-bound state can be best described as a conformational ensemble where zinc ion is co-ordinated with several combinations of histidine residues. As shown in Figure 1, close to the histidine residues, there are two carboxylate residues (E232 and D236) which may be potentially involved in zinc binding. We then made two mutants (E232S and D236S) and found that these mutations did not affect zinc-binding capacity of pZIP4–ECD (Supplementary Figure S1C), reinforcing the notion that zinc binding at the His-rich loop is primarily mediated by the four histidine residues.

## The His-rich loop is protease-susceptible and unstructured

During pZIP4–ECD purification, we noticed that the protein is highly vulnerable to proteolysis. We then used partial proteolysis and mass spectrometry to locate the most vulnerable region. As shown in Figure 3A, incubation of pZIP4–ECD with trypsin at a mass ratio of 300 : 1 (protein:protease) at room temperature for 20 min led to ~50% digestion of the full-length protein and incubation with more trypsin led to a fully processed and protease-resistant species with an apparent molecular mass of 24 kDa. ESI–TOF–MS analysis showed that the primary cleavage sites are all within the His-rich loop (Figure 3B). This result suggested that the His-rich loop must be most solvent exposed and largely unfolded so that the protease can reach and process it at a rate much higher than proteolysis at other potential cleavage sites. This deduction is consistent with the observation in the crystal structure of pZIP4–ECD where the His-rich loop is severely disordered, as well as the prediction by PSIPRED that the His-rich loop has no secondary structure. The highly superimposable CD spectra of the wild-type pZIP4–ECD and the 4HS mutant also supported that the histidine residues are not involved in secondary structure formation (Supplementary Figure S3).

## Zinc binding to the His-rich loop induces only minor and localized structural changes

Since the His-rich loop binds zinc ions, we are interested in examining the effects of zinc binding on the structure of pZIP4–ECD. We firstly compared the CD spectra of pZIP4–ECD in a zinc titration experiment. As shown in Supplementary Figure S4, addition of $ZnSO_4$ up to 24 μM to the apo form pZIP4–ECD (6 μM) did not lead to a significant change in spectrum. Adding zinc higher than 30 μM caused protein precipitation. Given the estimated binding affinities of pZIP4–ECD towards zinc ions (Supplementary Figure S1), the zinc-binding sites in the His-rich loop must have been saturated before protein precipitation. Therefore, the lack of CD spectrum change indicated that zinc binding to the His-rich loop did not affect the secondary structure of pZIP4–ECD.

We then tested whether zinc binding has any effect on the intrinsic fluorescence of pZIP4–ECD, which is a sensitive indicator of conformational changes. We found that although the peak wavelength of the fluorescence spectra (332 nm) was not shifted upon zinc binding, a

small but significant decrease in fluorescence intensity was observed (Figure 4A), suggestive of structural changes around the fluorophores. When excited at 295 nm, the fluorescence changes generally reflected the local environment changes of the tryptophan residues (W111, W262 and W289, Supplementary Figure S5). As W111 and W289 are buried in the N-terminal subdomain and the C-terminal subdomain, respectively, W262, which is immediately downstream of the His-rich loop, is most likely responsible for the decreased fluorescence intensity. To test whether zinc binding at the His-rich loop causes fluorescence decrease, we conducted the same zinc titration experiment on the 4HS mutant. As shown in Figure 4A,B, adding zinc only resulted in a small decrease in fluorescence intensity at 332 nm, confirming that zinc binding to the histidine residues is responsible for the decreased fluorescence intensity of the wild-type protein during titration.

If zinc binding greatly affects the structural and dynamic properties of the His-rich loop, a changed protease susceptibility would be expected. As shown in Figure 4C, zinc appears to partially protect pZIP4–ECD from proteolysis by trypsin, particularly when zinc concentration is at or higher than 20 μM, suggesting that zinc binding may slightly affect the structure of the His-rich loop and its surrounding residues. Collectively, the small intrinsic fluorescence change and the partial protective effect against proteolysis reflect a highly localized structural change induced by zinc binding to the His-rich loop.

## The His-rich loop plays a role in zinc transport of human ZIP4

Next, we examined the role of the clustered histidine residues in the His-rich loop for human ZIP4 (hZIP4) function. Because the amino acid sequence of the His-rich loop of pZIP4 has considerable similarity to its counterpart in hZIP4 (Figure 1B), we think the overall structural features and zinc-binding properties of pZIP4–ECD should be largely preserved in hZIP4. To test hZIP4 function, we conducted zinc uptake assay on hZIP4–HA (C-terminal HA tag) transiently expressed in HEK293T cells in the Chelex-treated cell culture media, rather than the zinc uptake buffer we used before [12,15]. Markedly, we found that the cells transfected with the empty vector absorbed much less radioactive $^{65}$Zn than the cells expressing hZIP4 (Supplementary Figure S6), resulting in a considerably reduced background level allowing for detection of a small change in zinc transport activity. We reasoned that the serum proteins in the Chelex-treated culture media sequestered zinc ions from solution [21,22], which suppressed zinc transport through HEK293T cells' endogenous zinc uptake systems much more than the overexpressed hZIP4. By using this approach, we compared the zinc uptake activities of the wild-type hZIP4 and the 4HS mutant (H238S/H241S/H243S/H245S). After calibration of zinc uptake activity using hZIP4–HA surface expression level, we found that the $V_{max}$ of the 4HS mutant decreased by ~20%, whereas the $K_m$ was not affected (Figure 5A). The cell surface expression level and the extent of glycosylation did not indicate any issue of misfolding and/or mistrafficking of the 4HS mutant.

Considering that the His-rich loop is right on the top of the transport entrance, it is plausible that it may function as an extracellular filter conducing a preselection of metal substrate. To test this, we firstly conducted zinc uptake assay in the presence of the excessive amount of several other divalent metal ions ($Ca^{2+}$, $Mg^{2+}$, $Co^{2+}$, $Ni^{2+}$, $Cu^{2+}$ and $Mn^{2+}$) (Figure 5B). The

results indicated that only non-radioactive $Zn^{2+}$ greatly and significantly reduced $^{65}Zn$ uptake, which is consistent with the notion that hZIP4 is a zinc-specific transporter. If the His-rich loop is contributive to zinc specificity by preselecting zinc ions over other metal ions, the 4HS mutant devoid of all the histidine residues would exhibit lower zinc transport activity in the presence of other metal ions. However, the result did not support this hypothesis as none of the tested metal ions, except for the non-radioactive $Zn^{2+}$, substantially reduced zinc transport activity.

Taken together, the functional characterization of the 4HS mutant suggested that the His-rich loop is involved in zinc transport but does not play a role in preselecting metal substrate.

## Discussion

The His-rich loop in the N-terminal ECD is a common feature of ZIP4, but so far there is no characterization of this loop except that it was shown to be severely disordered in the crystal lattice [12]. In this work, we found that the His-rich loop of pZIP4–ECD harbors at least two zinc-binding sites with low micromolar affinity (Figure 2 and Supplementary Figure S1). Biochemical and biophysical characterization showed that zinc binding at this protease-susceptible and highly dynamic loop only induces small and localized conformational changes (Figures 3 and 4). Mutagenesis and functional characterization indicated that the histidine residues in this loop play a role in zinc transport (Figure 5). These data allowed us to make a discussion in terms of the putative function of this loop.

The structural model of the full-length hZIP4 suggests the His-rich loop is right on the top of the TMD and appears to be in close proximity of the transport entrance (Figure 1A). Although the sequences of the His-rich loop are quite variable among ZIP4s (Figure 1B), the clustered histidine residues, probably together with the other neighboring metal chelating residues, likely confer a zinc-binding capability for all the ZIP4s, even though the number of zinc-binding site and/or binding affinities may vary depending on the exact sequence of the loop. Therefore, one putative function of the His-rich loop is to enrich zinc ions and increase effective zinc concentration at the pore entrance. However, the lack of change in the apparent $K_m$ of the 4HS mutation suggests that zinc enrichment by the His-rich loop does not contribute much to the overall affinity of hZIP4 towards zinc (Figure 5). As a matter of fact, deletion of the whole ECD (ΔECD) had no effect on the $K_m$ but drastically reduced the $V_{max}$ by 75%. A careful kinetic analysis of the 4HS mutant showed ~20% decrease in the $V_{max}$, partially accounting for the reduced $V_{max}$ of ΔECD. This result also excluded the possibility that the His-rich loop may play a role in inhibiting zinc transport. Such an inhibitory effect was reported in the study of a ZnT family member, MTP1 from *Arabidopsis thaliana* [23,24], where deletion of the cytosolic His-rich loop increased transport rate by more than 10 folds. Instead, the decreased transport rate of the 4HS mutant suggests that the His-rich loop may participate in zinc transport, presumably through the following two non-mutually exclusive mechanisms. For one, the loop may act as a chaperone facilitating zinc binding to the transport site in the TMD. Instead of acquiring free zinc ions from the extracellular space, the transport site may prefer accepting zinc ions already bound at the His-rich loop through rapid ligand exchange. The flexibility of the loop not only confers the transporter a more efficient way to capture zinc from the environment but also ensures a pool

of liable zinc, rather than immobilized zinc, available for the transporter. The similar chaperone mechanism has been proposed in the studies of zinc transporters ZnuA [25] and ZntA [26,27]. For the other mechanism, the His-rich loop may act as a zinc sensor allosterically regulating transporter's function. Although zinc binding only induces a small and highly localized conformational change, as indicated by the small change of tryptophan fluorescence intensity and partial protective effect against trypsin digestion (Figure 4), the His-rich loop is located at the 'bridging region' which was shown to be particularly important for ZIP4 trafficking and transport activity [12]. It is conceivable that even a small structural perturbation, such as that induced by zinc binding in the His-rich loop, may sufficiently affect transporter's activity. In contrast, the cytosolic His-rich loop of the ZIPs between the third and the fourth transmembrane helices appears to have distinct functions. It has been shown that the cytosolic His-rich loop of hZIP4 binds zinc ions with nanomolar affinity [28] and acts as an intracellular zinc sensor responsible for zinc-induced endocytic degradation of ZIP4 [29]. A recent study on a plant ZIP, IRT1 from *Arabidopsis thaliana*, suggested a metal sensing function of the corresponding His-rich loop essential for heavy metal-induced IRT1 ubiquitination and degradation [30]. This cytosolic His-rich loop was also reported to be associated with substrate specificity [31] and transport activity [29,32] for different ZIPs.

Sequence comparison of human ZIPs has revealed that, besides ZIP4, three other ZIPs also have a His-rich loop in their N-terminal ECDs. ZIP6 and ZIP10 were predicted to have a ZIP4-like extracellular dimerization subdomain [12], where the two proteins have a His-rich loop containing 27 and 40 histidine residues, respectively. The dimerization subdomain of ZIP7 appears to have degenerated, leaving 33 histidine residues in an unstructured loop exposed to the lumen of the ER. It was speculated that the N-terminal His-rich loop of ZIP7 may play a role in ER zinc homeostasis [33]. Nevertheless, the exact functions of these very long His-rich loops in ZIP6/ZIP7/ZIP10 have not been experimentally established. This work on ZIP4 will shed light on the research of these ZIPs, as well as many other metal transporters and metalloproteins with a similar His-rich segment.

## Conclusion

In this work, we focused our study on the extracellular His-rich loop by investigating its interactions with zinc ions and the importance of this unstructured, highly flexible loop for ZIP4 function. Our results indicated that zinc binding to the His-rich loop at the physiological zinc concentration only induces a small and localized structural perturbation. Mutagenesis and functional assays suggested that the histidine residues within this loop play a role in promoting zinc transport, but only to a small extent. In the study of ZnuA, when a functionally redundant ZinT protein was knocked out, the seemingly 'disposable' His-rich loop was demonstrated to be crucial for zinc acquisition in both *in vitro* and *in vivo* tests [34]. Whether the extracellular His-rich loop of ZIP4 is a part of the 'Plan B' to enhance zinc absorption under a stressful condition would be interesting to explore in the future study.

## Supplementary Material

Refer to Web version on PubMed Central for supplementary material.

## Funding

This work is supported by NIH [R01GM115373 and R01GM129004] (to J.H.).

## Abbreviations

| | |
|---|---|
| **AE** | Acrodermatitis Enteropathica |
| **CD** | circular dichroism |
| **DMEM** | Dulbecco's modified eagle medium |
| **DPBS** | Dulbecco's phosphate-buffered saline |
| **ECD** | extracellular domain |
| **ESI** | electrospray ionization |
| **ESI–TOF–MS** | time-of-flight mass spectrometer using electrospray ionization |
| **ZIP** | Zrt-/Irt-like protein |

## References

1. Jeong J and Eide DJ (2013) The SLC39 family of zinc transporters. Mol. Aspects Med 34, 612–619 10.1016/j.mam.2012.05.011 [PubMed: 23506894]
2. Lichten LA and Cousins RJ (2009) Mammalian zinc transporters: nutritional and physiologic regulation. Annu. Rev. Nutr 29, 153–176 10.1146/annurev-nutr-033009-083312 [PubMed: 19400752]
3. Liuzzi JP and Cousins RJ (2004) Mammalian zinc transporters. Annu. Rev. Nutr 24, 151–172 10.1146/annurev.nutr.24.012003.132402 [PubMed: 15189117]
4. Kambe T, Hashimoto A and Fujimoto S (2014) Current understanding of ZIP and ZnT zinc transporters in human health and diseases. Cell. Mol. Life Sci 71, 3281–3295 10.1007/s00018-014-1617-0 [PubMed: 24710731]
5. Li M, Zhang Y, Liu Z, Bharadwaj U, Wang H, Wang X et al. (2007) Aberrant expression of zinc transporter ZIP4 (SLC39A4) significantly contributes to human pancreatic cancer pathogenesis and progression. Proc. Natl Acad. Sci. U.S.A 104, 18636–18641 10.1073/pnas.0709307104 [PubMed: 18003899]
6. Lin Y, Chen Y, Wang Y, Yang J, Zhu VF, Liu Y et al. (2013) ZIP4 is a novel molecular marker for glioma. Neuro Oncol. 15, 1008–1016 10.1093/neuonc/not042 [PubMed: 23595627]
7. Ishida S, Kasamatsu A, Endo-Sakamoto Y, Nakashima D, Koide N, Takahara T et al. (2016) Novel mechanism of aberrant ZIP4 expression with zinc supplementation in oral tumorigenesis. Biochem. Biophys. Res. Commun 483, 339–345 10.1016/j.bbrc.2016.12.142 [PubMed: 28017725]
8. Weaver BP, Zhang Y, Hiscox S, Guo GL, Apte U, Taylor KM et al. (2010) Zip4 (Slc39a4) expression is activated in hepatocellular carcinomas and functions to repress apoptosis, enhance cell cycle and increase migration. PLoS ONE 5, e13158 10.1371/journal.pone.0013158 [PubMed: 20957146]

9. Wang K, Zhou B, Kuo YM, Zemansky J and Gitschier J (2002) A novel member of a zinc transporter family is defective in Acrodermatitis Enteropathica. Am. J. Hum. Genet 71, 66–73 10.1086/341125 [PubMed: 12032886]
10. Küry S, Dréno B, Bézieau S, Giraudet S, Kharfi M, Kamoun R et al. (2002) Identification of SLC39A4, a gene involved in Acrodermatitis Enteropathica. Nat. Genet 31, 239–240 10.1038/ng913 [PubMed: 12068297]
11. Dufner-Beattie J, Weaver BP, Geiser J, Bilgen M, Larson M, Xu W et al. (2007) The mouse Acrodermatitis Enteropathica gene Slc39a4 (Zip4) is essential for early development and heterozygosity causes hypersensitivity to zinc deficiency. Hum. Mol. Genet 16, 1391–1399 10.1093/hmg/ddm088 [PubMed: 17483098]
12. Zhang T, Sui D and Hu J (2016) Structural insights of ZIP4 extracellular domain critical for optimal zinc transport. Nat. Commun 7, 11979 10.1038/ncomms11979 [PubMed: 27321477]
13. Wang F, Kim BE, Dufner-Beattie J, Petris MJ, Andrews G and Eide DJ (2004) Acrodermatitis Enteropathica mutations affect transport activity, localization and zinc-responsive trafficking of the mouse ZIP4 zinc transporter. Hum. Mol. Genet 13, 563–571 10.1093/hmg/ddh049 [PubMed: 14709598]
14. Kambe T and Andrews GK (2009) Novel proteolytic processing of the ectodomain of the zinc transporter ZIP4 (SLC39A4) during zinc deficiency is inhibited by Acrodermatitis Enteropathica mutations. Mol. Cell. Biol 29, 129–139 10.1128/MCB.00963-08 [PubMed: 18936158]
15. Zhang T, Liu J, Fellner M, Zhang C, Sui D and Hu J (2017) Crystal structures of a ZIP zinc transporter reveal a binuclear metal center in the transport pathway. Sci. Adv 3, e1700344 10.1126/sciadv.1700344 [PubMed: 28875161]
16. Antala S, Ovchinnikov S, Kamisetty H, Baker D and Dempski RE (2015) Computation and functional studies provide a model for the structure of the zinc transporter hZIP4. J. Biol. Chem 290, 17796–17805 10.1074/jbc.M114.617613 [PubMed: 25971965]
17. Lin W, Chai J, Love J and Fu D (2010) Selective electrodiffusion of zinc ions in a Zrt-, Irt-like protein, ZIPB. J. Biol. Chem 285, 39013–39020 10.1074/jbc.M110.180620 [PubMed: 20876577]
18. Krężel A and Maret W (2007) Dual nanomolar and picomolar Zn(II) binding properties of metallothionein. J. Am. Chem. Soc 129, 10911–10921 10.1021/ja071979s [PubMed: 17696343]
19. Bauer MC, Nilsson H, Thulin E, Frohm B, Malm J and Linse S (2008) $Zn^{2+}$ binding to human calbindin $D_{28k}$ and the role of histidine residues. Protein Sci. 17, 760–767 10.1110/ps.073381108 [PubMed: 18359862]
20. Bafaro EM, Maciejewski MW, Hoch JC and Dempski RE (2019) Concomitant disorder and high-affinity zinc binding in the human zinc- and iron-regulated transport protein 4 intracellular loop. Protein Sci. 28, 868–880 10.1002/pro.3591 [PubMed: 30793391]
21. Wang F, Kim BE, Petris MJ and Eide DJ (2004) The mammalian Zip5 protein is a zinc transporter that localizes to the basolateral surface of polarized cells. J. Biol. Chem 279, 51433–51441 10.1074/jbc.M408361200 [PubMed: 15322118]
22. Kirschke CP and Huang L (2003) Znt7, a novel mammalian zinc transporter, accumulates zinc in the Golgi apparatus. J. Biol. Chem 278, 4096–4102 10.1074/jbc.M207644200 [PubMed: 12446736]
23. Kawachi M, Kobae Y, Mimura T and Maeshima M (2008) Deletion of a histidine-rich loop of AtMTP1, a vacuolar $Zn^{2+}/H^{+}$ antiporter of *Arabidopsis thaliana*, stimulates the transport activity. J. Biol. Chem 283, 8374–8383 10.1074/jbc.M707646200 [PubMed: 18203721]
24. Tanaka N, Kawachi M, Fujiwara T and Maeshima M (2013) Zinc-binding and structural properties of the histidine-rich loop of Arabidopsis thaliana vacuolar membrane zinc transporter MTP1. FEBS Open Bio. 3, 218–224 10.1016/j.fob.2013.04.004
25. Banerjee S, Wei B, Bhattacharyya-Pakrasi M, Pakrasi HB and Smith TJ (2003) Structural determinants of metal specificity in the zinc transport protein ZnuA from synechocystis 6803. J. Mol. Biol 333, 1061–1069 10.1016/j.jmb.2003.09.008 [PubMed: 14583199]
26. Mitra B and Sharma R (2001) The cysteine-rich amino-terminal domain of ZntA, a Pb(II)/Zn(II)/Cd(II)-translocating ATPase from Escherichia coli, is not essential for its function. Biochemistry 40, 7694–7699 10.1021/bi010576g [PubMed: 11412123]

27. Banci L, Bertini I, Ciofi-Baffoni S, Finney LA, Outten CE and O'Halloran TV (2002) A new zinc-protein coordination site in intracellular metal trafficking: solution structure of the Apo and Zn(II) forms of ZntA(46–118). J. Mol. Biol 323, 883–897 10.1016/S0022-2836(02)01007-0 [PubMed: 12417201]

28. Bafaro EM, Antala S, Nguyen TV, Dzul SP, Doyon B, Stemmler TL et al. (2015) The large intracellular loop of hZIP4 is an intrinsically disordered zinc binding domain. Metallomics 7, 1319–1330 10.1039/C5MT00066A [PubMed: 25882556]

29. Mao X, Kim BE, Wang F, Eide DJ and Petris MJ (2007) A histidine-rich cluster mediates the ubiquitination and degradation of the human zinc transporter, hZIP4, and protects against zinc cytotoxicity. J. Biol. Chem 282, 6992–7000 10.1074/jbc.M610552200 [PubMed: 17202136]

30. Dubeaux G, Neveu J, Zelazny E and Vert G (2018) Metal sensing by the IRT1 transporter-receptor orchestrates its own degradation and plant metal nutrition. Mol. Cell 69, 953–964 e955 10.1016/j.molcel.2018.02.009 [PubMed: 29547723]

31. Nishida S, Mizuno T and Obata H (2008) Involvement of histidine-rich domain of ZIP family transporter TjZNT1 in metal ion specificity. Plant Physiol. Biochem 46, 601–606 10.1016/j.plaphy.2008.02.011 [PubMed: 18434175]

32. Milon B, Wu Q, Zou J, Costello LC and Franklin RB (2006) Histidine residues in the region between transmembrane domains III and IV of hZip1 are required for zinc transport across the plasma membrane in PC-3 cells. Biochim. Biophys. Acta Biomembr 1758, 1696–1701 10.1016/j.bbamem.2006.06.005

33. Adulcikas J, Norouzi S, Bretag L, Sohal SS and Myers S (2018) The zinc transporter SLC39A7 (ZIP7) harbours a highly-conserved histidine-rich N-terminal region that potentially contributes to zinc homeostasis in the endoplasmic reticulum. Comput. Biol Med 100, 196–202 10.1016/j.compbiomed.2018.07.007 [PubMed: 30029049]

34. Petrarca P, Ammendola S, Pasquali P and Battistoni A (2010) The Zur-regulated ZinT protein is an auxiliary component of the high-affinity ZnuABC zinc transporter that facilitates metal recruitment during severe zinc shortage. J. Bacteriol 192, 1553–1564 10.1128/JB.01310-09 [PubMed: 20097857]

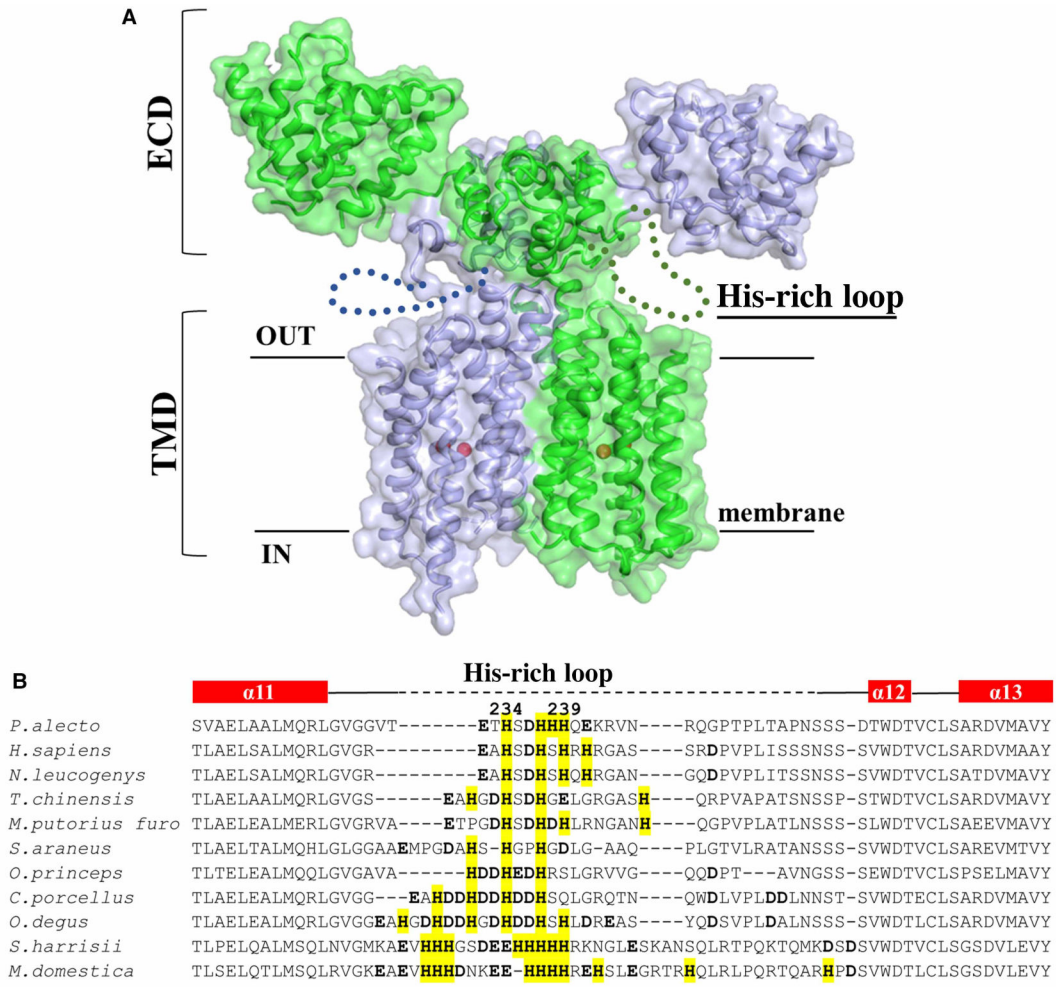


**Figure 1. The His-rich loop in ZIP4–ECD.**

(**A**) Structural model of the full-length human ZIP4 homodimer. The model was built based on structures of the pZIP4–ECD and a prokaryotic ZIP [12,15]. The dimerization interface of the TMD was adapted from a computational model of human ZIP4 with minor manual adjustment [16]. The protein is shown in both cartoon mode and surface mode. The metal ions bound at the transport site are depicted as red balls. The unstructured His-rich loops are drawn as dotted lines. The length of the His-rich loop is roughly proportional to the number of amino acid residues. (**B**) Sequence alignment of the His-rich loops from closely related mammalian ZIP4s. The potential metal chelating residues within the loop are in bold and the histidine residues are highlighted. The secondary structure of pZIP4–ECD is shown on the top of the alignment. The first and the last histidine residues in the His-rich loop of pZIP4 are numbered.

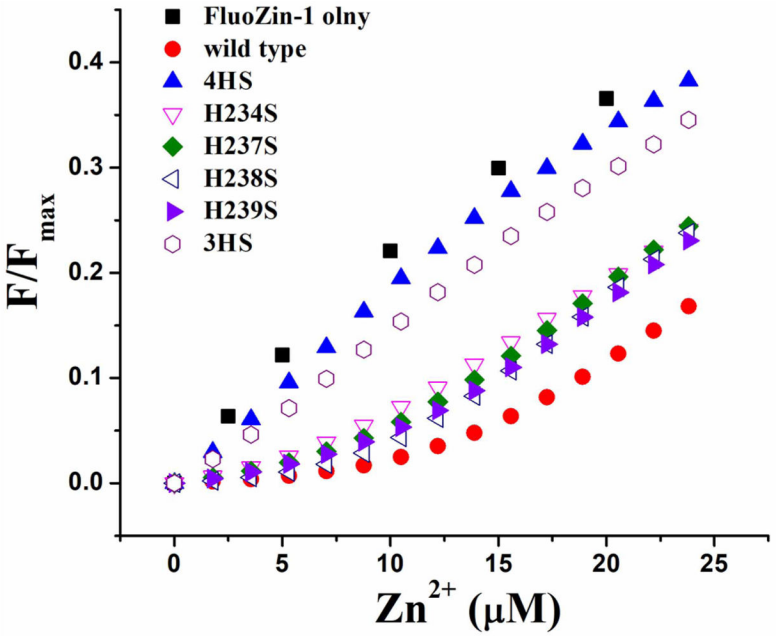


**Figure 2. Zinc binding to pZIP4–ECD.**

FluoZin-1 (5 μM) was titrated by $ZnCl_2$ in the absence and presence of pZIP4–ECD or the His-rich loop mutants (10 μM). The apparent zinc binding affinities were estimated and shown in Supplementary Figure S1B.

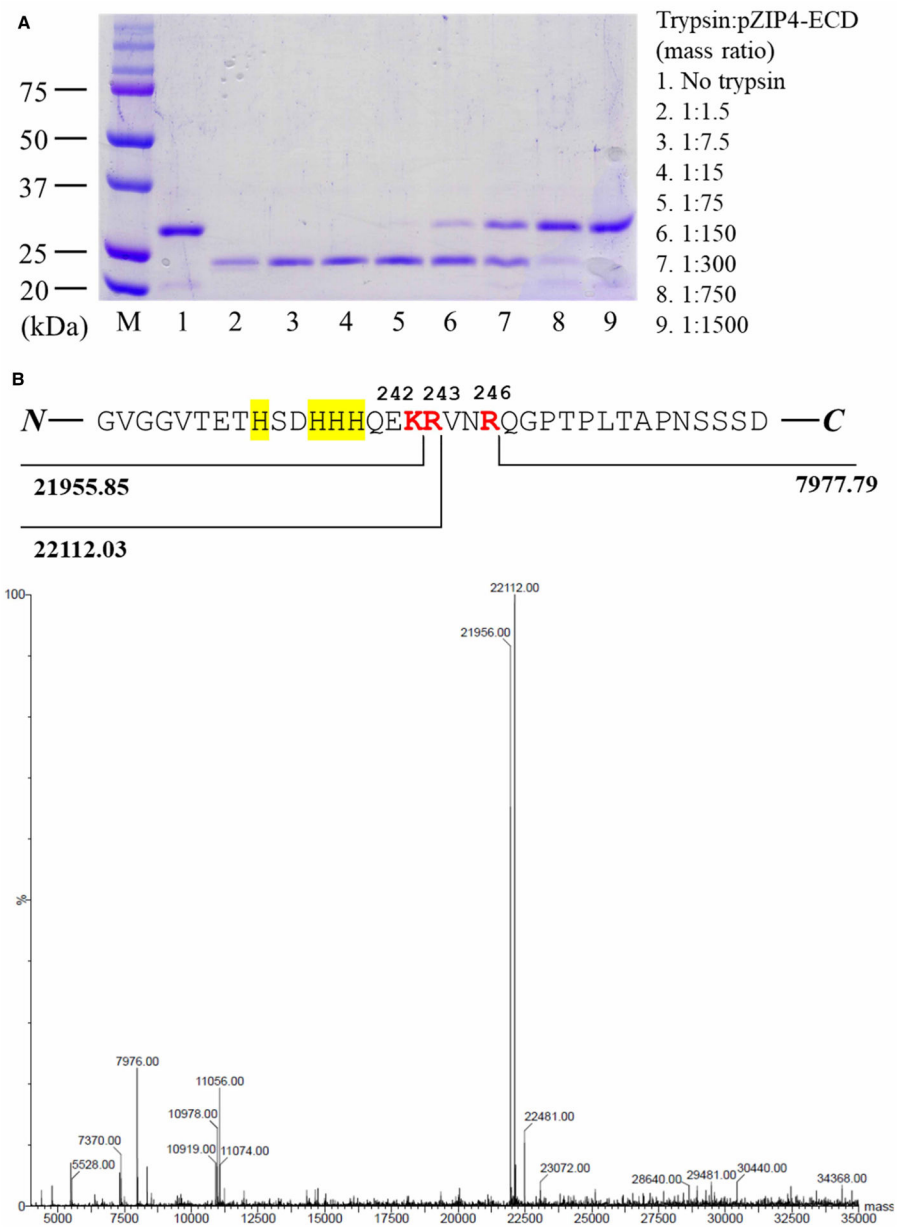


**Figure 3. Proteolysis of pZIP4–ECD by trypsin.**

(**A**) pZIP4–ECD proteolysis by indicated amount of trypsin. The concentration of pZIP4–ECD is 0.15 mg/ml (5 μM). The trypsin band (~24 kDa) could be overlapped with the proteolytic products in SDS–PAGE. (**B**) ESI–TOF–MS spectrum of the fully processed pZIP4–ECD by trypsin (sample 5 in (**A**)). The assigned fragments are underlined in the spectrum. The determined cleavage sites in the His-rich loop are colored in red. Note that the disulfide bonds within each fragment have been considered in the calculation of the theoretical average molecular mass.

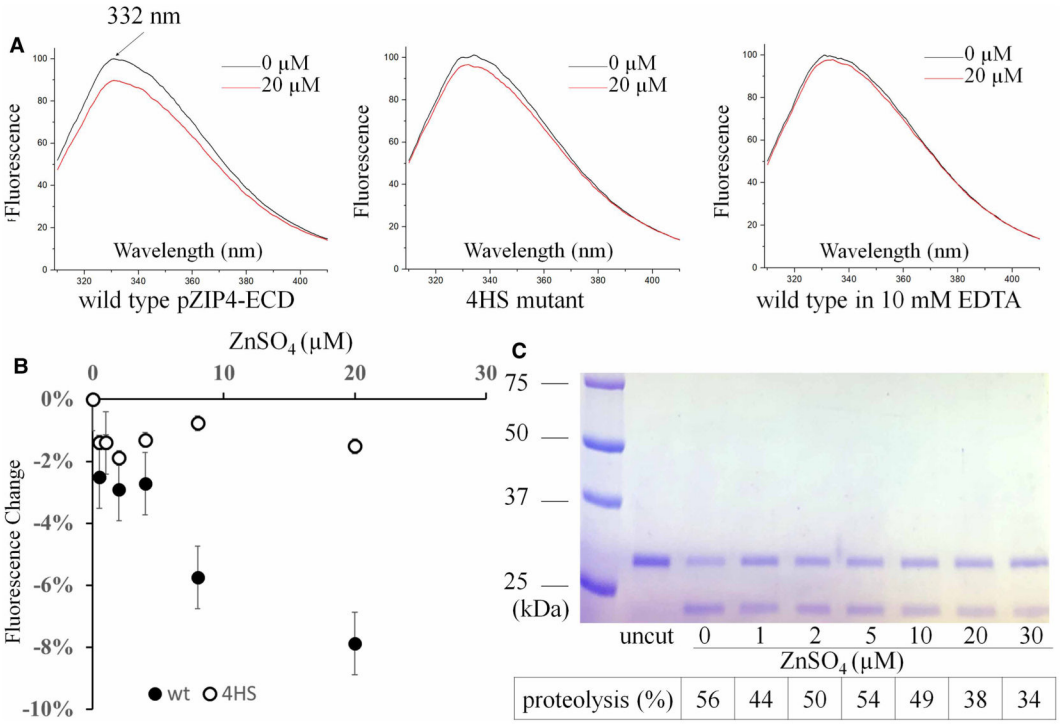


**Figure 4. Detection of zinc-induced conformational change of pZIP4–ECD.**

(**A**) Fluorescence spectra of pZIP4–ECD and the 4HS mutant in the absence and presence of zinc. (**B**) Fluorescence intensity changes at 332 nm of the wild-type protein and the 4HS mutant during zinc titration. Non-specific effect of zinc ion on fluorescence (the third panel in (**A**)) was subtracted. (**C**) Partial proteolysis of pZIP4–ECD (6 μM) in the presence of zinc sulfate at the indicated concentrations. Trypsin was added at the mass ratio of 300 : 1 (pZIP4–ECD:protease). Proteolysis was quantified and shown as a percentage below each lane.

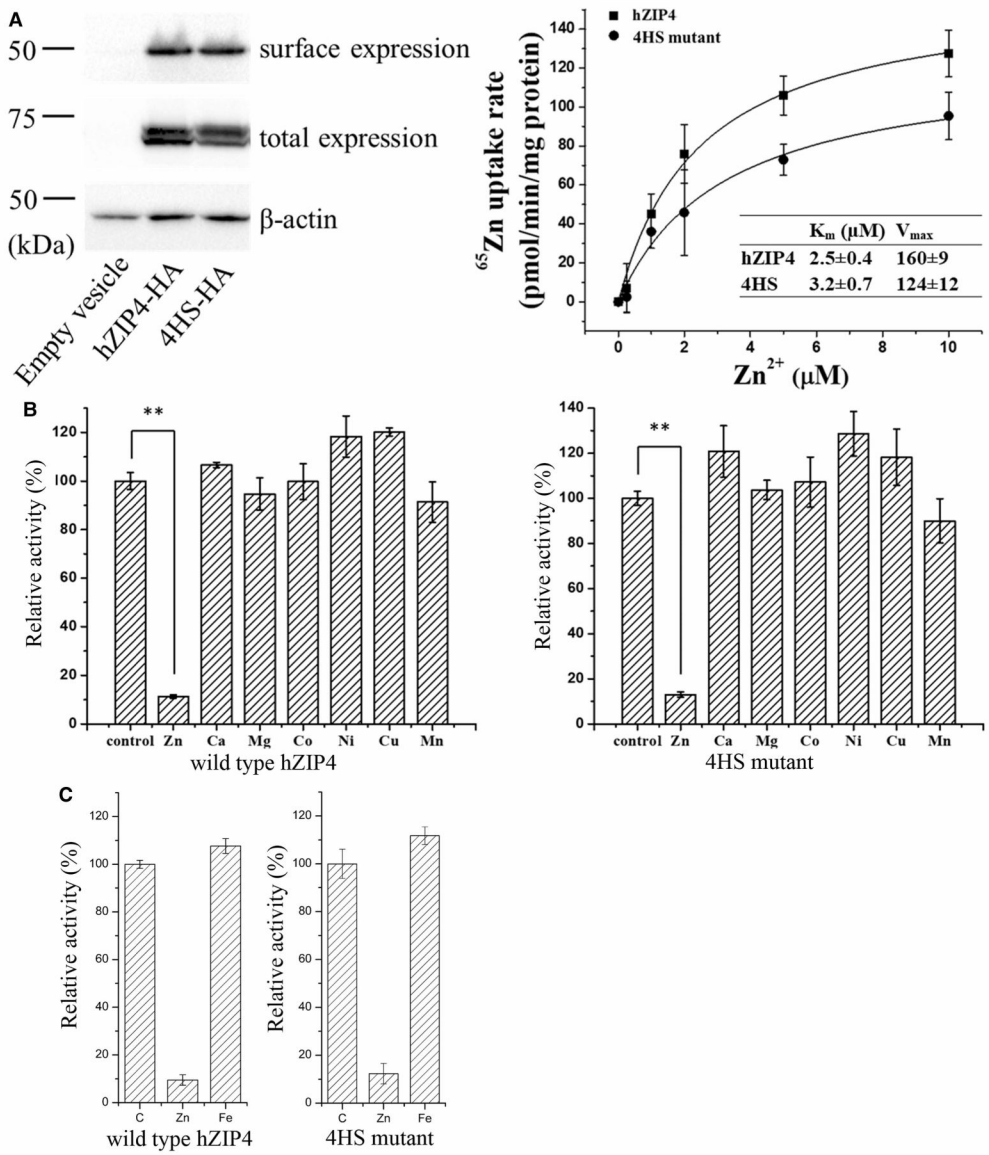


**Figure 5. Functional characterization of the His-rich loop in hZIP4.**

(**A**) Zinc uptake assays of the wild-type hZIP4–HA and the 4HS mutant transiently expressed in HEK293T cells. *Left:* Western blots showing the cell surface expression level (determined by surface-bound anti-HA antibody) and the total protein expression level of hZIP4 and the 4HS mutant. The upper band of total expression indicated the glycosylated form of hZIP4. *Right:* The processed zinc uptake data and curve fitting of one representative experiment. The kinetics parameters are shown in the inserted table. The $V_{max}$ values have been calibrated using the surface expression levels shown in the left. ** $P < 0.01$. (**B**) Zinc uptake through hZIP4 and the 4HS mutant in the absence and presence of non-radioactive zinc and other divalent metal ions in excess. 10 μM $^{65}$Zn was used in this assay and the concentrations of other metal ions are listed below. Non-radioactive $Zn^{2+}$: 200 μM; $Ca^{2+}$: 2 mM; $Mg^{2+}$: 20 mM; $Co^{2+}$: 200 μM; $Ni^{2+}$: 200 μM; $Cu^{2+}$: 200 μM; and $Mn^{2+}$: 200 μM. ** *P*

< 0.01. (**C**) Zinc uptake through hZIP4 and the 4HS mutant in the presence of 200 μM ferrous ($Fe^{2+}$) and 1 mM ascorbic acid.